Development of an Empirical Correlation for Ethanol Jet in Crossflow Spray Profiles in Transonic and Supersonic Flows

Aubrey J. McKelvy[1], James Braun[1], Guillermo Paniagua[1], Etienne Choquet[2], Thierry André[2], François Falempin[2]

Abstract

The complexity of two-phase interactions in the atomization process has resulted in the use of empirical correlations for the determination of spray features relevant to engine designers. This paper details the development of a correlation for liquid ethanol spray penetration from a plain-orifice injector with experimental validity across both the transonic and supersonic crossflow regimes. Penetration heights and spray transmittance are measured in a 23x17x54 cm linear test section with crossflow Mach numbers ranging from 0.3 to 0.8. Contoured 2D converging-diverging nozzles are inserted into the bottom of the test section to produce supersonic flow with a conically expanding flow path providing Mach 2 crossflows at the injector. An analytical derivation for a momentum flux ratio correction factor is used to collapse penetration heights across both the subsonic and supersonic regimes. The correlation utilizes a physics-based form to account for both near-field (x/d 0-50) and far-field (x/d 50-200) spray patterns that power-law correlations fail to capture. The performance of the correlation is finally compared to a selection of published correlations that are valid for similar flow conditions.

Keywords: Jet-in-Crossflow, Spray-Correlation, Penetration-Depth, Transonic-Flow, Supersonic-Flow

Nomenclature

A	Fast Fourier transform amplitude	x	Axial coordinate (m)
a	Acceleration (m/s^2)	$\bar{x}$	Nondimensional axial coordinate
C_D	Drag coefficient	y	Transverse coordinate (m)
D	Drag force (N)	$\bar{y}$	Nondimensional transverse coordinate
d	Injector diameter (m)	μ	Dynamic viscosity ($Pa\ s$)
d_l	Droplet diameter (m)	ρ	Density (kg/m^3)
Fr	Froude number	σ	Surface tension (N/m)
f	Frequency (Hz)		
g	Gravitational acceleration ($m/s\text{^}2$)	Subscripts	
J	Momentum flux ratio	a	Crossflow properties
l_c	Characteristic length	i	Arbitrary component
M	Mach number	l	Injectant properties
$\dot{m}$	Mass flow (kg/s)	o	Total properties
P	Pressure (Pa)	r	Relative velocity
R	Coefficient of determination	x	Axial component
Re	Reynolds number	y	Transverse component
SMD	Sauter Mean Diameter (m)		
St	Stokes number		
T	Temperature (K)		
t	Time (s)		
u	Velocity (m/s)		
We	Weber number		

---

[1] *Maurice J. Zucrow Laboratories, Purdue University, West Lafayette, IN, USA*
[2] *MBDA, Le Plessis Robinson, France*

HiSST-2024-153
Development of an Empirical Correlation for Ethanol Jet in Crossflow
Spray Profiles in Transonic and Supersonic Flows

Page | 1

1. Introduction

Transverse liquid injection through plain orifice injectors is a simple and effective multiphase mixing strategy for high-speed gaseous crossflows and falls under the broad classification of jets in crossflow (JIC) [1]. This class of flows has become an active area of aerospace research with early applications in temperature and flow control, specifically within air-breathing propulsion systems [2] [3]. Liquid JIC (LJIC) has primarily been utilized as a fuel mixing scheme but has similarly been used for temperature control in turbo-jet compressors [4] [5]. The primary advantage offered by LJIC over other atomization techniques is superior penetration and mixing in high momentum crossflows by taking advantage of air-blast atomization, and while the applications are more niche than traditional turbo-jet fuel injection schemes, there has been increasing research interest in LJIC in both high-subsonic and supersonic flows.

A key statistic in the performance of LJIC systems is spray penetration depth, and a variety of diagnostic techniques have been employed in its measurement. The most common is light extinction, being used in early studies of supersonic LJIC by Schetz et al. [6] [7] and extensively in more recent studies by Lin et al. [8] and Obenauf et al. [9]. Extinction techniques make use of back-lighting to image the spray's shadow (often at high frequencies) to give a measure of transmittance, allowing the spray profile to be measured. The simplest system is 'back-lit imaging', making use of any number of diffuse light sources, but schlieren visualization techniques (including shadowgraphy) are more commonly used due to improved background quality and their ability to visualize density gradients in the crossflow. Laser sheet Mie-scattering and phase doppler interferometry have also been used to evaluate penetration depth, but these have produced results inconsistent with extinction techniques due to incompatible definitions of the spray edge [10].

The impingement of the crossflow on the liquid jet creates inherently three-dimensional flow structures, and the varied droplet sizes and breakup characteristics produce inconsistent drag forces throughout the spray. These complexities make analytical modelling of spray penetration exceedingly difficult. While there has been significant progress in computational modelling of LJIC with the advent of Eulerian dispersed phase modelling [11] and volume of fluid approaches [12] [13], system designers still rely on empirical correlations generated from relevant experimental datasets. A recent review of subsonic LJIC penetration correlations was presented by Wang et al. [14], listing more than 30 penetration correlations. Supersonic correlations are comparatively scarce but have been presented by Kush and Schetz [7], Lin et al. [10], Ghenai et al. [15], and Beloki Perurena et al. [16].

Despite the large number of correlations represented by these works, their applicability is limited to narrow ranges of crossflow conditions, and most of them are purely phenomenological. The goal of this study is to produce a physics-based correlation with experimental validation across a wide variety of crossflows and to present an alternate method for the calculation of relevant nondimensional numbers to enable coalescence of penetration data at arbitrary supersonic Mach numbers.

2. Methods

The experimental data featured in this study were collected in the PT1 wind tunnel at the Purdue Experimental Turbine Aerothermal Laboratory (PETAL) [17]. This section details the experimental facilities, diagnostic techniques, and data processing used to compile the statistics.

2.1. Experimental Facilities

PT1 is a blowdown type wind tunnel operating with a 56 cubic meter air reservoir with a 135 bar peak capacity. Air flow is regulated with two Valtek Mark 100 Globe Control Valves, one of which passes air through a large heat exchanger allowing temperatures exceeding 600 K, and metered through a critical venturi before introduction into the PT1 settling chamber via radial discharge; a bypass line allows the airflow conditions to be stabilized before the tunnel is charged. Fig. 1 shows a diagram of the wind tunnel equipped for LJIC experiments. The settling chamber reduces the turbulence intensity and length scales with two fine mesh screens and a honeycomb array before the flow is contracted into the 23 by 17 cm profile of the test section. The downstream reservoir is a 500 cubic meter vacuum tank providing back pressures ranging from ambient to as low as 5 Torr.
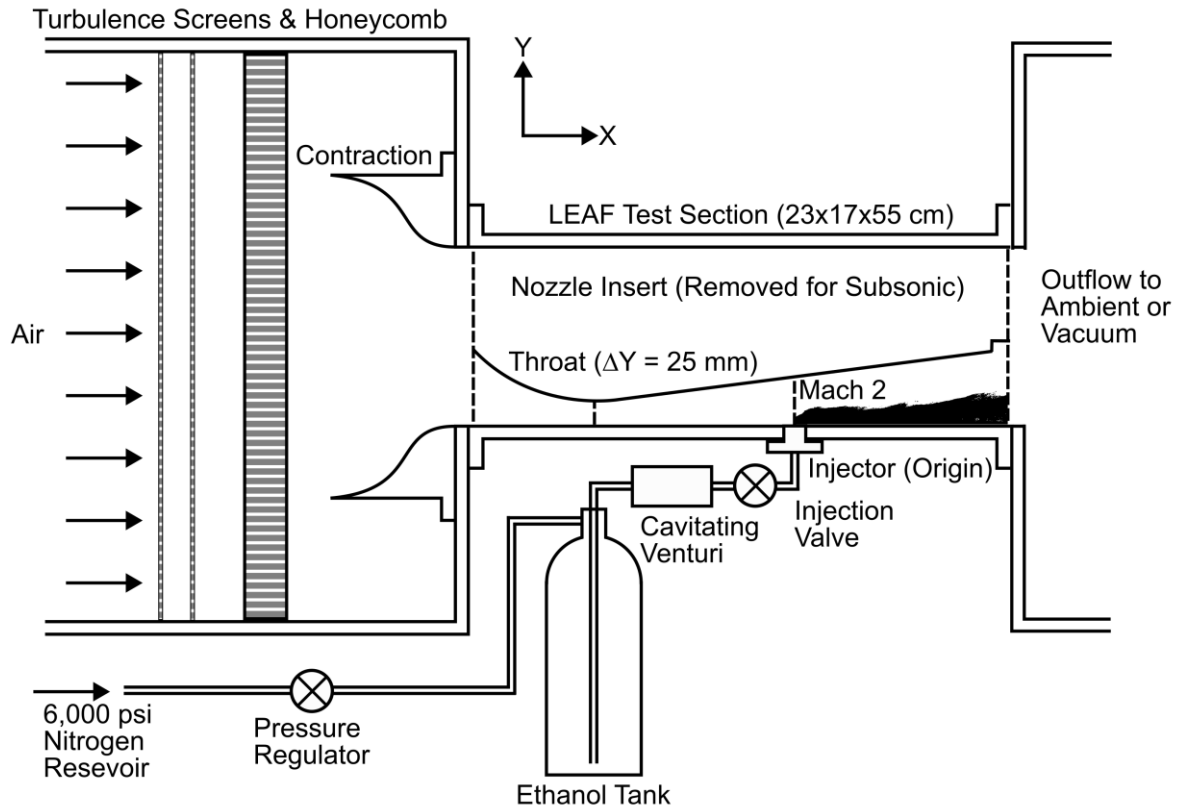
HiSST-2024-153
Development of an Empirical Correlation for Ethanol Jet in Crossflow
Spray Profiles in Transonic and Supersonic Flows

Page | 2

Copyright © 2024 by author(s)

Fig. 1. A schematic of the PT1 wind tunnel configured for LJIC experiments.

The test section allows a range of subsonic Mach numbers to be generated in its open configuration, but it can also accommodate supersonic crossflows by restricting the flow path with contoured nozzle inserts. The contour shown in Fig. 1 generates a Mach 2 crossflow at the injector. Plain orifice injectors of 0.5, 1, and 2 mm with a 12 mm channel length are flush mounted 28 cm downstream of the test section inlet and allow the transverse injection of ethanol. Injection pressures are regulated from a 400 bar nitrogen reservoir and liquid mass flows are metered through a cavitating venturi.

2.2. Diagnostics

Pressure and temperature are measured at various points in the wind tunnel to generate crossflow statistics. Pressure is measured with a combination of Scanivalve Digital Sensor Arrays (DSA), Scanivalve Miniature Pressure Scanners (MPS), and Druck PMP-1260 Industrial Pressure Transmitters; temperature is measured with K-type thermocouples via a VTI Instruments EX1048A conditioning system. The pressure transducers and thermocouples are regularly calibrated in house with a Druck DPI612 pressure calibrator and a Fluke Calibration 9172 Field Metrology Well, respectively. An instrumented flush mounted insert on the upstream side of the injection plate allows a Kiel probe and thermocouple to be submerged to characterize the total pressure and temperature of the crossflow along with a static pressure measurement. The pressure distribution within the flow field is characterized by an array of pressure taps along the contoured surface and a set of axial taps along the injection plate. Kulite XCE-062 pressure transducers are also used to measure high frequency (250 kHz) pressure fluctuations near the injector. Figure 2 shows time-traces of relevant measurements for a typical test along with diagrams of the sensor locations and a comparison between experiment and a Reynolds Averaged Navier-Stokes (RANS) computation.

HiSST-2024-153
Development of an Empirical Correlation for Ethanol Jet in Crossflow
Spray Profiles in Transonic and Supersonic Flows
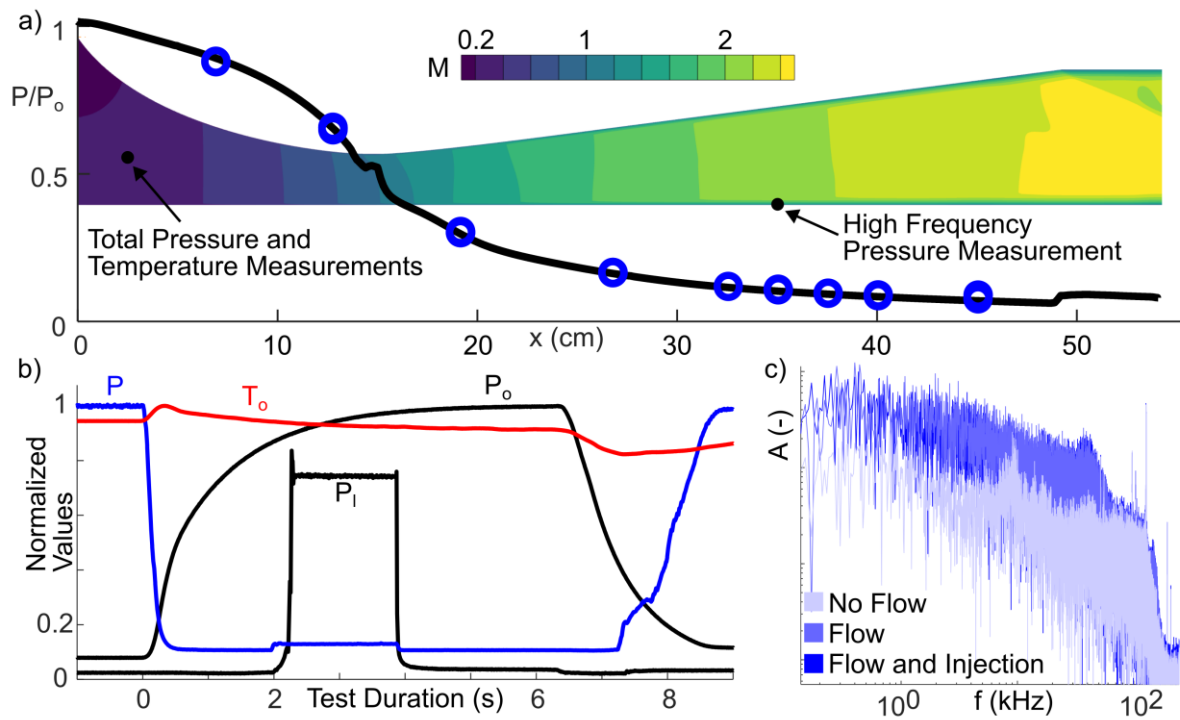
Page | 3

Copyright © 2024 by author(s)

Figure 2. A Mach contour of the supersonic flow path and a comparison of simulated and experimental pressure ratios (a), a time series of normalized experimental statistics (b), and an FFT of pressure fluctuations (c).

The test section sidewalls are composed of large quartz windows that enable optical access across the entire flow field. The spray penetration is characterized in this study with a combination of backlit imaging, shadowgraphy, and schlieren employed as extinction techniques. A Phantom TMX 5010 high-speed camera is used to collect images with acquisition rates ranging from 20 to 50 kHz. Background images are taken of the flow before and after liquid injection and used to compute transmittance through the spray. A 90% transmittance threshold is a commonly used definition for spray penetration [18] and is employed in this study. Figure 3 shows a comparison of penetration heights measured using the three different extinction techniques and an example of instantaneous and averaged spray images with 90% and 50% transmittance boundaries overlayed. Additionally, a transmittance contour banded in intervals of 10% is shown.

HiSST-2024-153
Development of an Empirical Correlation for Ethanol Jet in Crossflow
Spray Profiles in Transonic and Supersonic Flows
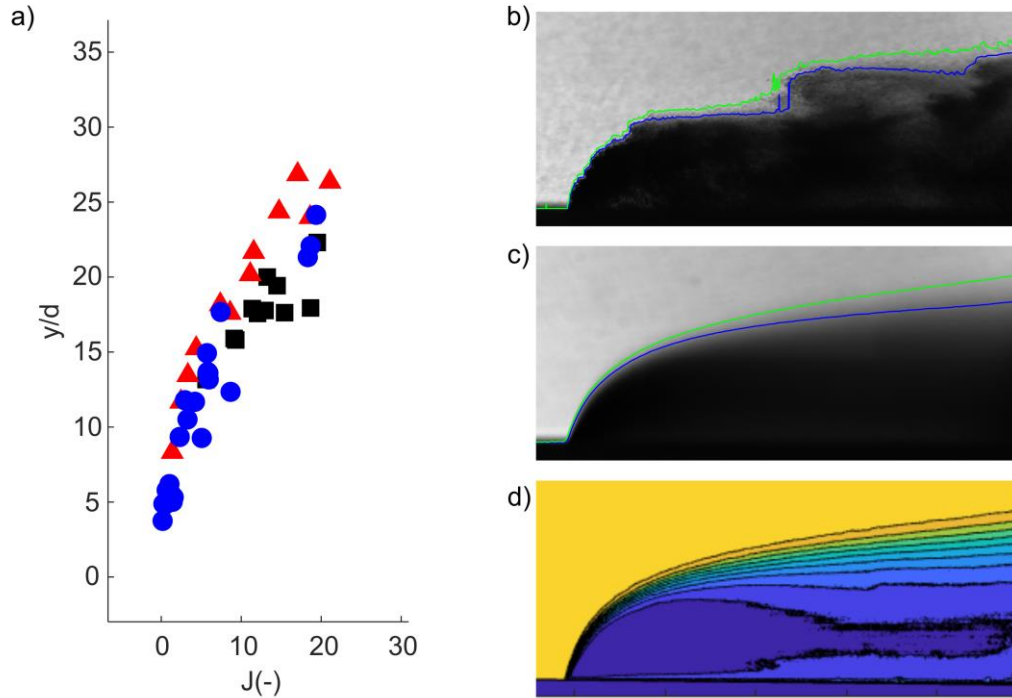
Page | 4

Copyright © 2024 by author(s)

Figure 3. A plot of 90% transmittance penetration heights at x/d = 55 for different optical techniques (a) and a snapshot (b), average image (c), and transmittance contour (d) of a J=1.74 spray in a Mach 0.64 crossflow.

The penetration heights in Figure 3 are plotted with respect to the momentum flux ratio, a commonly used statistic for collapsing LJIC penetration heights.

$$J = \frac{\rho_l u_l^2}{\rho_a u_a^2} \tag{1}$$

The cavitating venturi is calibrated with a Coriolis flow meter and allows liquid mass flows to be directly measured. Gauge pins are used to precisely determine injector orifice diameters and enable the calculation of injectant velocity. This removes any dependence of relevant statistics on injector discharge coefficients, which can vary with cavitation number [19].

A Monte Carlo method is employed to estimate two-sigma confidence intervals for the experimental statistics. A detailed description of the implementation is given by McKelvy et al. [20], and table 1 lists typical statistics and their associated two-sigma bounds.

Table 1. Condition bounds and associated two-sigma confidence intervals.

	M	$\dot{m}_a$	P	T_o	Re	We
Minimum	0.2378 ± 0.0086	2.45 ± 0.1	23.9 ± 0.24	250 ± 1.2	2,820	170
Maximum	1.9562 ± 0.0064	11.98 ± 0.05	100.2 ± 0.2	501 ± 2.5	50,510	5,700

2.3 Derivation of the Model Form

Two spray correlations are presented in this study: one is generated with the commonly used 'power law' form while the other uses a form based on a derivation for droplet transport. The crossflows included in this study feature high momentum flux, producing very high aerodynamic Weber numbers. This leads to extremely rapid primary and secondary breakup, resulting in a droplet cloud very near the injector exit. This motivates the use of a trajectory analysis on a spherical droplet to choose the form

HiSST-2024-153
Development of an Empirical Correlation for Ethanol Jet in Crossflow
Spray Profiles in Transonic and Supersonic Flows

Page | 5

Copyright © 2024 by author(s)

of the spray penetration correlation. The effects of the precise location of secondary breakup and the droplet sizes along the 90% transmittance boundary on the spray penetration are accounted for by empirical coefficients in Section 3.3. Additionally, the high air velocities and small particle sizes result in droplet dynamics dominated by inertial forces, allowing gravitational acceleration to be neglected if the Froude number is much greater than unity (Froude numbers in this study range from 800 to 9,000).

The drag force on a spherical droplet can be expressed with the following equation.

$$D = \frac{C_D}{8}\rho_a u_r^2 \pi d_l^2 \qquad (2)$$

The subscript a indicates crossflow properties, u_r is the velocity of the droplet relative to the crossflow, and d_l is the droplet diameter. Accounting for the mass of a spherical liquid droplet gives the following formulation for the component-wise acceleration.

$$a_i = -\frac{3\rho_a C_D u_r u_i}{4\rho_l d_l} \approx -\frac{3\rho_a C_D u_x u_i}{4\rho_l d_l} \qquad for\ u_x \gg u_y \qquad (3)$$

The subscript i represents either the x or y directions, and the subscript l indicates liquid properties. The dependence of the relative velocity on both the x and y velocity components results in a system of non-linear differential equations that is extremely tedious to solve. Implicit solutions are possible [21], but they result in complex formulations. To generate a simpler form, the x component (associated with the crossflow velocity) is assumed to be much larger than the y component (associated with the injection velocity); this allows the implementation of the small angle approximation and gives $u_r \approx u_x$. The other terms in equation 3 are assumed constant and will be used to nondimensionalize x and y with the following expression.

$$\frac{\bar{x}}{x/d} = \frac{\bar{y}}{y/d} = l_c = \frac{3\rho_a C_D}{4\rho_l} \qquad (4)$$

Here the bars indicate nondimensionalized coordinates, and the scaling term is named the characteristic length (l_c). Note that the subscript on the droplet diameter is dropped; d represents the injector diameter and is used in the remainder of this study for computing l_c. This change is primarily for convenience of data processing and of use of the correlation. Integrating equation 3 gives the following expressions for the time-dependent velocity components.

$$u_x(t) = u_a - \left(\frac{1}{u_a} + \frac{l_c t}{d}\right)^{-1}$$

$$u_y(t) = \frac{u_l}{u_a}\left(\frac{1}{u_l} + \frac{l_c t}{d}\right)^{-1} \qquad (5)$$

Here u_a is the crossflow mean axial velocity at the injector, and u_l is the injection velocity. Integrating again and eliminating t gives the following expression for $\bar{x}$ as a function of $\bar{y}$.

$$\bar{x} = \exp\left(\frac{u_a}{u_l}\bar{y}\right) - \frac{u_a}{u_l}\bar{y} \qquad (6)$$

Equation 5 can be solved for $\bar{y}$ with the Lambert W function to finally give the form of the correlation.

$$\bar{y} = \frac{u_l}{u_a}\left(-W_{-1}\left(-\exp(-(\bar{x}+1))\right) - (\bar{x}+1)\right) \qquad (7)$$

Here the subscript (-1) indicates the branch of the Lambert W function.

3. Results

3.1. Bulk Data

Figure 4 shows 90% transmittance spray penetration boundaries for all the cases investigated in this study. There are 87 cases; 30 of these feature subsonic crossflows (plotted in black) and 57 feature supersonic crossflows (plotted in red). The trajectories span a variety of axial locations up to a maximum of 270 diameters, and momentum flux ratios vary from 0.17 to 180.
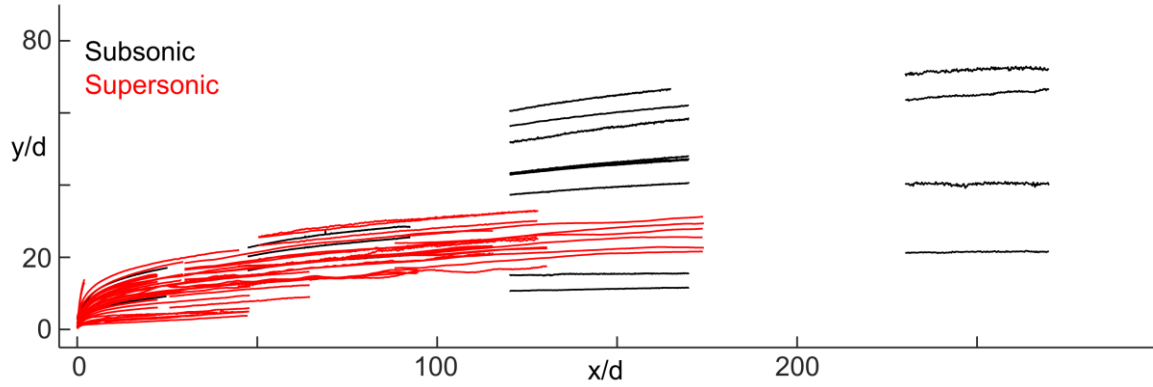
HiSST-2024-153
Development of an Empirical Correlation for Ethanol Jet in Crossflow
Spray Profiles in Transonic and Supersonic Flows

Page | 6

Copyright © 2024 by author(s)

Figure 4. A plot of all 90% transmittance spray edges extracted with supersonic cases indicated in red and subsonic in black.

Figure 5a plots penetration heights at various distances against the momentum flux ratio. There is a well cited monotonic increase in spray penetration with increasing momentum flux ratio but also a discontinuity in the trend, with smaller exponential growth observed in the high J cases. This is related to the crossflow Mach number, with the shallower trend relating to subsonic cases and the steeper trend at low J relating to supersonic crossflows.
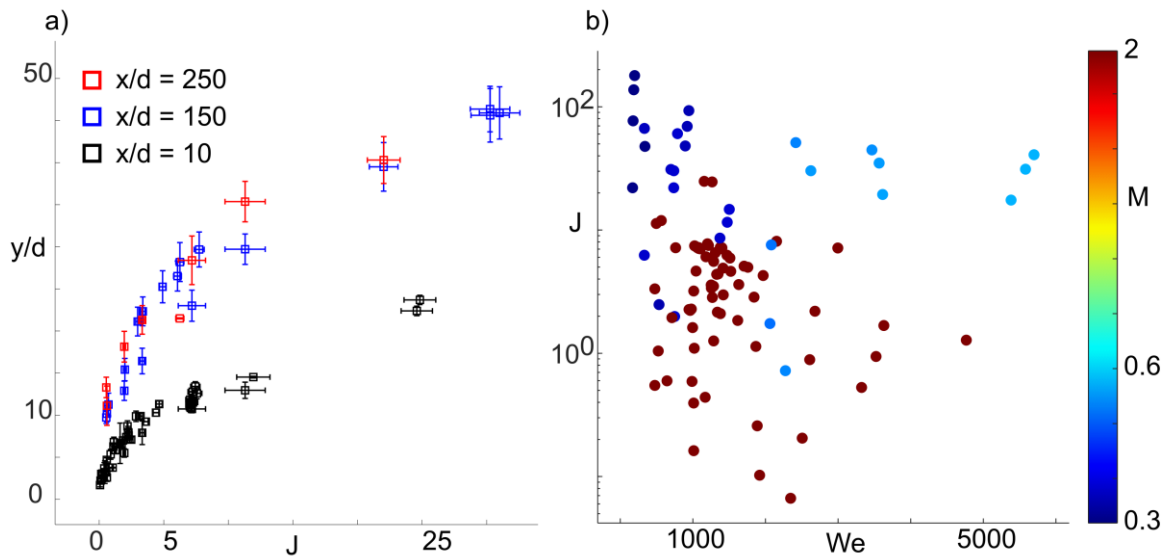

Figure 5. A plot of penetration heights with respect to momentum flux ratio at different axial locations (a) and a mapping of all the conditions included in this study with respect to Weber number and momentum flux ratio.

Figure 4 also highlights the inability for momentum flux ratio to collapse penetration heights of cases with differing crossflow properties, with discrepancies beyond 7 diameters at the same momentum flux ratio and axial distance. Variations in crossflow density and temperature and in liquid temperature will affect the droplet size distribution and trajectories but are not entirely captured in the momentum flux ratio. Droplet size distributions are characterized by mean diameters and have been shown to scale inversely with Reynolds and Weber numbers [22].

$$Re = \frac{\rho_a u_r d}{\mu_a} \qquad\qquad We = \frac{\rho_a u_r^2 d}{\sigma} \qquad (8)$$

In this study, both numbers are defined with the relative crossflow velocity with respect to the initial injection velocity ($u_r = \sqrt{u_a^2 + u_l^2}$) and μ_a and σ are the crossflow dynamic viscosity and liquid surface tension, respectively. Additionally, the Froude and Stokes numbers characterize droplet dynamics more

HiSST-2024-153
Development of an Empirical Correlation for Ethanol Jet in Crossflow
Spray Profiles in Transonic and Supersonic Flows

Page | 7

Copyright © 2024 by author(s)

directly, with the Froude number accounting for the relative effect of gravitational acceleration (as previously mentioned) and the Stokes number accounting for the inertia of the droplets.

$$Fr = \frac{u_r}{\sqrt{gd}} \qquad St = \frac{\rho_l d_l^2}{18\mu_l} \approx 76 \frac{d\rho_l Re^{0.2}}{\rho_a We^{0.8}} \qquad (9)$$

The formulation for Stokes number only accounts for Stokes drag (a condition requiring low Reynolds crossflows) and so only gives a qualitative scaling; the actual Stokes numbers for the conditions in this study will be much lower than those computed with the formulation in equation 9 due to the addition of non-viscous drag effects. Additionally, the dependence of St on particle diameters is satisfied with a correlation for the Sauter Mean Diameter (SMD) for high Reynolds LJIC generated by Ingebo [22], this gives the approximate formulation shown in equation 9. Figure 6 shows the distribution of these four dimensionless numbers within the investigated dataset.
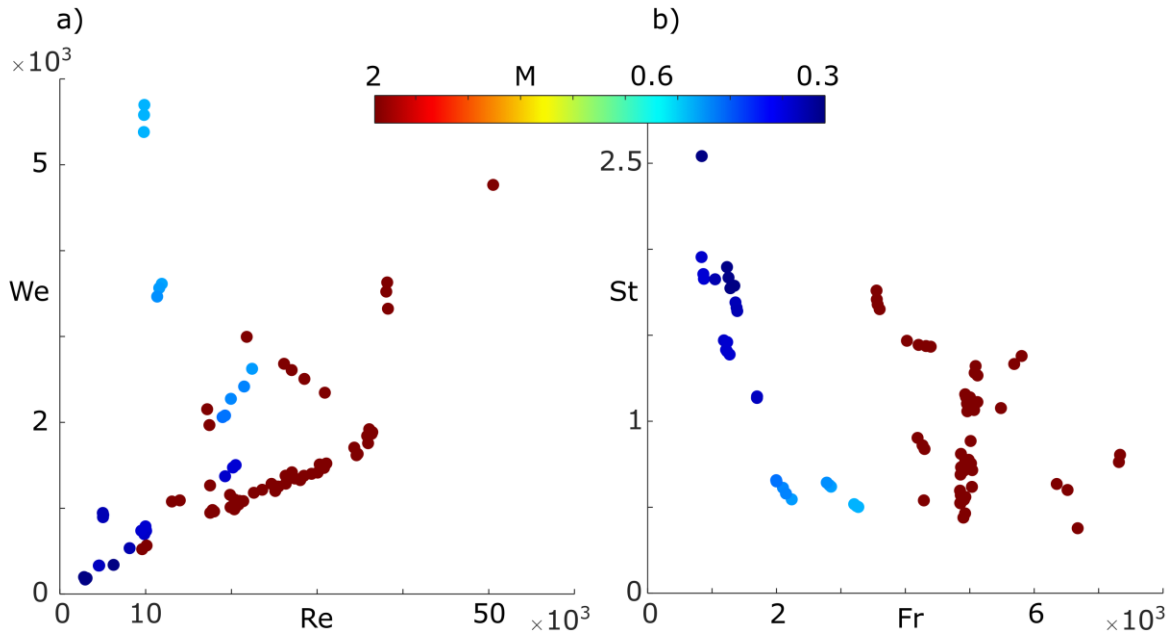

Figure 6. Scatter plots of Reynolds and Weber numbers (a) and of Stokes and Froude numbers (b).

A summary of the range of flow properties included in this study is provided in Table 2.

Table 2. Ranges of relevant flow properties used in the generation of the spray penetration correlation.

	M	J	Re	We	Fr	$P[kPa]$	$T_o[K]$	$l_c[m^{-1}]$
Minimum	0.238	0.173	2,820	170	835	23.9	251	0.242
Maximum	1.96	179	50,500	5,700	7,330	100	502	1.31

These values represent the range of experimental conditions that the penetration correlations are validated against and includes both subsonic and supersonic crossflows.

3.2. Corrections

The attempt to collapse subsonic and supersonic spray penetrations presented in this study relies on an estimation of crossflow properties downstream of the bow shock that forms on the windward side of the liquid jet. Figure 7a shows a shadowgraph image featuring a typical spray bow shock and Figure 7b shows a contour of pixel intensity standard deviation (with darker pixels indicating highly varying pixel intensity) that highlights the location and range of motion exhibited by both the shock and the

HiSST-2024-153
Development of an Empirical Correlation for Ethanol Jet in Crossflow
Spray Profiles in Transonic and Supersonic Flows

Page | 8

Copyright © 2024 by author(s)

spray edge. The bow shock forms a complex three-dimensional surface around the spray and varies with the instabilities and droplet packets that form on the windward edge of the jet, with large lumps in the jet forming corresponding contours in the shock profile. The bow shock remains closely attached to the liquid jet from the injector until the point where the penetration profile has the largest curvature; the central-plane shock angle along this portion varies from 0 degrees at the boundary layer to roughly 35 degrees at the point of separation and 40 degrees in the far-field. Incorporating a model for flow velocities and angles behind the bow shock is beyond the scope of this work, however the relatively small shock angles present close to the injector motivates the use of normal shock relations to estimate the properties of the airflow that initially impinges the jet.
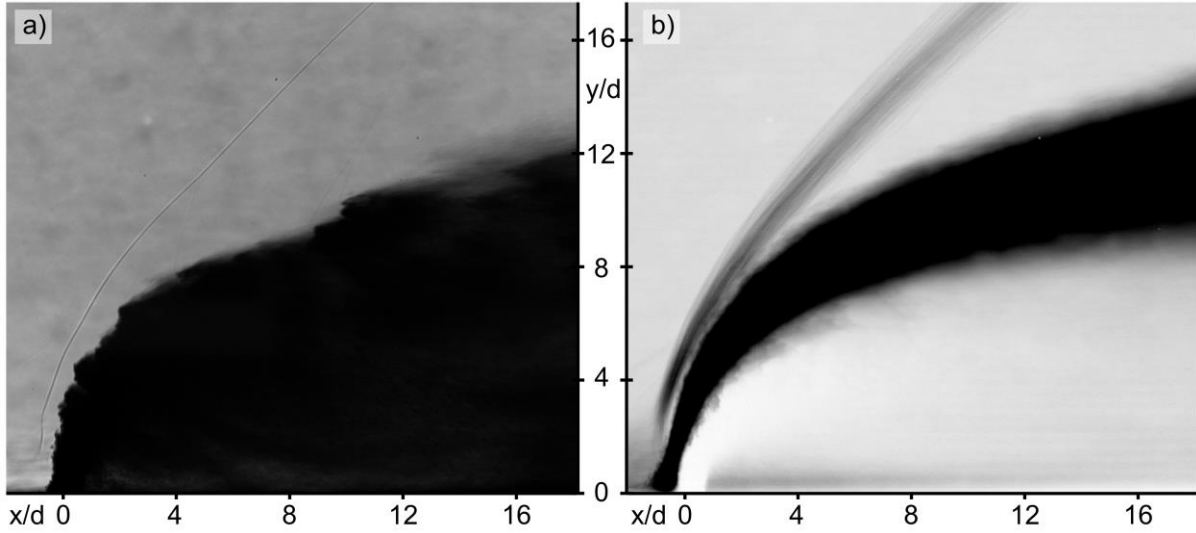

Figure 7. A shadowgraph snapshot of a J = 3.2 spray in a Mach 2 crossflow (Re = 27,000, We = 4,500) (a), and a contour of pixel standard deviation showing ranges of bow shock and spray edge variation.

This correction is applied to all relevant statistics used in the correlation fitting, namely crossflow velocity, density, and temperature, all of which impact the non-dimensional numbers and characteristic length. An analytical expression for the momentum flux ratio with this correction is given by the following equation.

$$\frac{J_{sub}}{J_{sup}} = \frac{(\gamma + 1)M^2}{(\gamma - 1)M^2 + 2} = 2.6 \tag{10}$$

Here γ is the ratio of specific heats (taken as 1.4 in this study), and the subscripts sub and sup indicate the 'corrected' subsonic momentum flux ratio and the 'uncorrected' supersonic momentum flux ratio, respectively. With the Mach 1.96 crossflow present in this study, this correction requires multiplying J by 2.6. An additional consideration is the value of the drag coefficient in equation 4 and the droplet diameter in equation 9. The previously mentioned correlation for Sauter mean diameter by Ingebo [22] is used along with a correlation for drag coefficient at Reynolds numbers greater than 1,000 presented by Desantes et al. [23].

$$\frac{SMD}{d} = 37(ReWe)^{-0.4} \qquad\qquad C_D = 0.44 \tag{11}$$

3.3. Correlation

The derivation presented in section 2.3 and the discussion of nondimensional numbers in section 3.1 motivate the use of the following statistics to model spray penetration.

$$\frac{y}{d} = f(\frac{x}{d}, l_c, J, Re, We, Fr, St) \tag{12}$$

HiSST-2024-153
Development of an Empirical Correlation for Ethanol Jet in Crossflow
Spray Profiles in Transonic and Supersonic Flows

Page | 9

Copyright © 2024 by author(s)

The inclusion of J accounts for the ratio u_l/u_a in the derivation of the correlation form, and all these statistics except x/d are changed by applying normal shock relations to the supersonic crossflows.

A Levenberg-Marquardt nonlinear least squares algorithm [24] is used to fit the model form to the experimental penetration profiles. The resulting correlation is given as follows.

$$\bar{y} = 0.59 J^{0.44} Re^{-0.1} We^{0.13} Fr^{-0.53} St^{-0.32} \left(-W_{-1}\left(-\exp\left(-(\bar{x}^{0.58} + 1) \right) \right) - (\bar{x}^{3.3} + 1) \right) \qquad (13)$$

A correlation using the widely used but phenomenological power law form is also generated to evaluate the relative performance of the trajectory-based form and the inclusion of nondimensional numbers beyond the momentum flux ratio.

$$\frac{y}{d} = 1.58 J^{0.46} \left(\frac{x}{d} \right)^{0.34} \qquad (14)$$

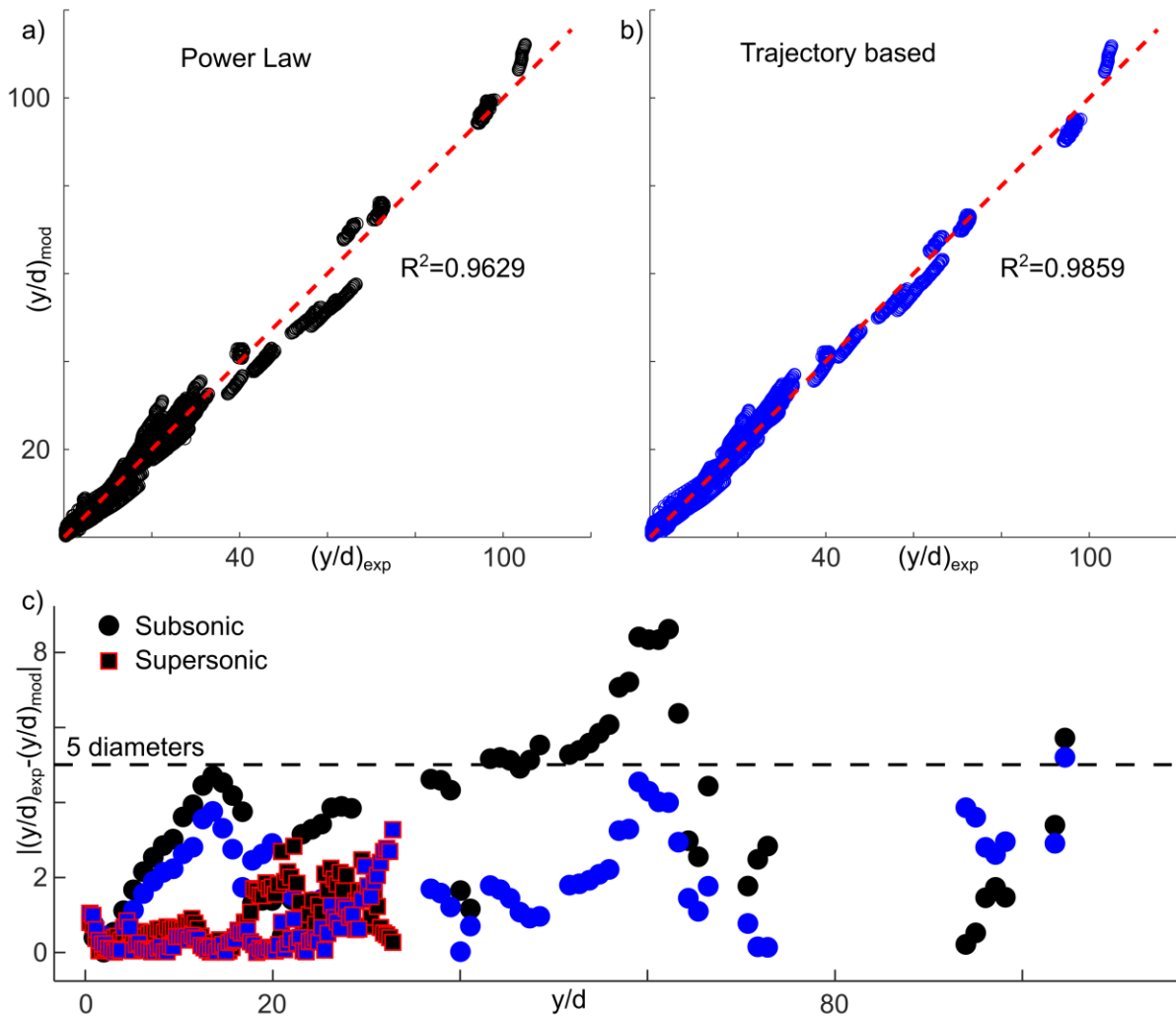The performance of these two correlations is shown in Figure 8.

Figure 8. Plots comparing correlation penetration heights with respect to measured penetration heights for the power law form (a) and the trajectory-based form (b), and a plot of the absolute difference between correlation and measured heights.

Both correlation forms provide reasonable performance, though both also make use of the Mach corrected momentum flux ratio. The trajectory-based has better matching with the experimental profiles, giving a coefficient of determination (R) of 98.6%, a 2.3% increase over the power law form. Subfigure c plots the absolute difference between the experimental profiles and the correlation. The largest errors for both forms occur in subsonic profiles at penetration depths around 60 diameters, but

HiSST-2024-153
Development of an Empirical Correlation for Ethanol Jet in Crossflow
Spray Profiles in Transonic and Supersonic Flows

Page | 10

Copyright © 2024 by author(s)

the trajectory-based correlation has roughly half the error seen in the power law. The most significant deviations are seen in two specific subsonic profiles: one close to the injector between 0 and 20 diameters and a second at the highest y/d. Both feature very high momentum flux ratios and begin to violate the $u_a \gg u_l$ assumption utilized in the form derivation. Most of the experimental profiles are matched within +/- 1 diameter within 20 diameters of penetration, and the trajectory-based correlation matches all profiles within +/- 5 diameters (excepting the highest penetration case).

Figure 9 plots the trajectory-based correlation for an arbitrary case with $J = 10$ against the correlations presented by Lin et al. [10] ($M = 1.94$), Ghenai et al. [15] ($M = 1.5$), Beloki Perurena et al. [16] ($M = 6$), and a subsonic correlation also presented by Lin et al. [25].
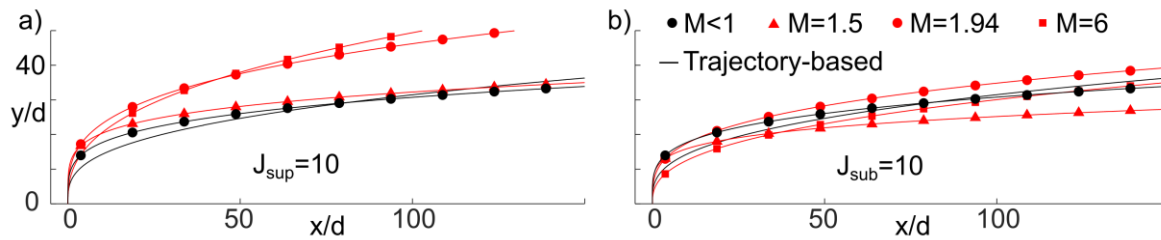

Figure 9. Comparisons of the trajectory-based correlation at $J = 10$ with unmodified published correlations (a) and with Mach corrected momentum flux ratios (b).

Subfigure a shows that the trajectory-based correlation matches Lin et al.'s subsonic correlation well, especially in the far-field. Unsurprisingly, the correlations generated on supersonic data do not match well as, with the conventional calculation of supersonic momentum flux ratios, the momentum flux of the liquid jet is considerably larger for the same J than in a subsonic crossflow. Subfigure b plots the same correlations, but with the Mach correction provided by equation 10 applied to all the supersonic correlations and produces a much tighter grouping. This highlights another key advantage of the normal-shock approximation employed on the crossflow properties in this study: it allows the existing literature on supersonic spray penetration correlations to make predictions at different Mach numbers and allows subsonic spray experiments to inform injector performance at supersonic Mach numbers.

4. Conclusion

A dataset of 90% transmittance spray penetration profiles of ethanol jets through plain-orifice injectors was collected across a wide variety of subsonic and supersonic crossflows at various pressures and temperatures, and a novel correlation form was derived from first principles. Corrections were proposed to the calculation of the common set of nondimensional scaling parameters (employing the normal shock relations) resulting in coalescence of subsonic and supersonic spray penetrations. The combination of these numbers and the novel correlation form resulted in a correlation for spray penetration that performed better than the commonly used power law. The correlation had experimental validity between Mach 0.3 and Mach 2 and between 0 and 150 diameters downstream of the injector with less than 5 diameters of deviation between experiment and correlation. Finally, an elegant formulation for the Mach corrected momentum flux ratio was presented and shown to collapse penetration correlations generated by other researchers at Mach numbers ranging from 1.5 to 6 with subsonic correlations.

References

[1]   A. R. Karagozian, "The jet in crossflow," *Physics of Fluids*, vol. 26, no. 10, 2014.
[2]   E. E. Callaghan and R. S. Ruggeri, "Investigation of the penetration of an air jet directed perpendicularly to an air stream," National Advisory Committee for Aeronautics, Cleveland, Ohio, 1948.
[3]   E. E. Callaghan and D. T. Bowden, "Investigation of flow coefficient of circular, square, and elliptical orifices at high pressure ratios," 1949.
[4]   L. J. Chelko, "Penetration of liquid jets into a high-velocity air stream," 1950.

HiSST-2024-153
Development of an Empirical Correlation for Ethanol Jet in Crossflow
Spray Profiles in Transonic and Supersonic Flows

Page | 11

Copyright © 2024 by author(s)

[5]   D. B. Fenn, "Correlation of isothermal contours formed by penetration of jet of liquid ammonia directed normal to an airstream," 1954.

[6]   A. Sherman and J. Schetz, "Breakup of liquid sheets and jets in a supersonic gas stream," *AIAA Journal*, vol. 9, no. 4, pp. 666–673, 1971.

[7]   E. A. Kush Jr and J. A. Schetz, "Liquid jet injection into a supersonic flow," *AIAA Journal*, vol. 11, no. 9, pp. 1223–1224, 1973.

[8]   K.-C. Lin, T. Ombrello, and C. D. Carter, "Qualitative study of near-field and cross-sectional structures of liquid jets in supersonic crossflow," in *2018 AIAA Aerospace Sciences Meeting*, 2018, p. 0671.

[9]   D. Obenauf, J. Braun, T. Meyer, G. Paniagua, P. Sojka, and F. Falempin, "Characterization of the steady and unsteady spray structures of a liquid jet in supersonic crossflow," *International Conference on Liquid Atomization and Spray Systems (ICLASS)*, vol. 1, no. 1, 2021, doi: 10.2218/iclass.2021.6157.

[10]   K.-C. Lin, P. Kennedy, and T. Jackson, "Structures of water jets in a Mach 1.94 supersonic crossflow," in *42nd AIAA Aerospace Sciences Meeting and Exhibit*, 2004, p. 971.

[11]   H. Liu, Y. Guo, and W. Lin, "Numerical simulations of spray jet in supersonic crossflows using an Eulerian approach with an SMD model," *International Journal of Multiphase Flow*, vol. 82, pp. 49–64, 2016, doi: 10.1016/j.ijmultiphaseflow.2016.03.003.

[12]   L. Zhu *et al.*, "Numerical investigation of scale effect of various injection diameters on interaction in cold kerosene-fueled supersonic flow," *Acta Astronaut*, vol. 129, pp. 111–120, 2016, doi: 10.1016/j.actaastro.2016.09.001.

[13]   J. Zhao, C. Yan, L. Wu, W. Lin, Y. Tong, and W. Nie, "Numerical simulation of single/double liquid jets in supersonic crossflows," *Aerosp Sci Technol*, vol. 120, p. 107289, 2022, doi: 10.1016/j.ast.2021.107289.

[14]   M. Wang, M. Broumand, and M. Birouk, "LIQUID JET TRAJECTORY IN A SUBSONIC GASEOUS CROSS-FLOW: AN ANALYSIS OF PUBLISHED CORRELATIONS," *Atomization and Sprays*, vol. 26, no. 11, pp. 1083–1110, 2016, doi: 10.1615/atomizspr.2016013485.

[15]   C. Ghenai, H. Sapmaz, and C.-X. Lin, "Penetration height correlations for non-aerated and aerated transverse liquid jets in supersonic cross flow," *Exp Fluids*, vol. 46, pp. 121–129, 2009.

[16]   J. Beloki Perurena, C. O. Asma, R. Theunissen, and O. Chazot, "Experimental investigation of liquid jet injection into Mach 6 hypersonic crossflow," *Exp Fluids*, vol. 46, no. 3, pp. 403–417, 2008, doi: 10.1007/s00348-008-0566-5.

[17]   G. Paniagua *et al.*, "Design of the Purdue experimental turbine aerothermal laboratory for optical and surface aerothermal measurements," *J Eng Gas Turbine Power*, vol. 141, no. 1, p. 012601, 2019.

[18]   K.-C. Lin, M.-C. Lai, T. Ombrello, and C. D. Carter, "Structures and temporal evolution of liquid jets in supersonic crossflow," in *55th AIAA aerospace sciences meeting*, 2017, p. 1958.

[19]   W. H. Nurick, "Orifice cavitation and its effect on spray mixing," 1976.

[20]   A. J. McKelvy, J. Braun, G. Paniagua, T. Andre, E. Choquet, and F. Falempin, "Quantitative Definition of Spray Edge With Extinction Diagnostics and Evaluation of Attenuation Coefficient for Liquid Jets in Supersonic Crossflow," *J Eng Gas Turbine Power*, vol. 146, no. 6, 2024.

[21]   G. W. Parker, "Projectile motion with air resistance quadratic in the speed," *Am. J. Phys*, vol. 45, no. 7, pp. 606–610, 1977.

[22]   R. D. Ingebo, "Capillary and acceleration wave breakup of liquid jets in axial-flow airstreams," 1981.

[23]   J. M. Desantes, X. Margot, J. M. Pastor, M. Chavez, and A. Pinzello, "CFD− phenomenological diesel spray analysis under evaporative conditions," *Energy & Fuels*, vol. 23, no. 8, pp. 3919–3929, 2009.

[24]   G. A. F. Seber and C. J. Wild, "Nonlinear regression. hoboken," *New Jersey: John Wiley & Sons*, vol. 62, no. 63, p. 1238, 2003.

[25]   K.-C. Lin, P. Kennedy, and T. Jackson, "Penetration heights of liquid jets in high-speed crossflows," in *40th AIAA Aerospace Sciences Meeting & Exhibit*, 2002, p. 873.

HiSST-2024-153
Development of an Empirical Correlation for Ethanol Jet in Crossflow
Spray Profiles in Transonic and Supersonic Flows

Page | 12

Copyright © 2024 by author(s)